Available online at www.sciencedirect.com

ScienceDirect

journal homepage: www.elsevier.com/locate/issn/15375110

Research Paper

CFD and weighted entropy based simulation and optimisation of Chinese Solar Greenhouse temperature distribution

Xin Zhang [a], Hongli Wang [a], Zhirong Zou [a,**], Shaojin Wang [b,c,*]

[a] College of Horticulture, Northwest A&F University, Yangling, Shaanxi 712100, China
[b] College of Mechanical and Electronic Engineering, Northwest A&F University, Yangling, Shaanxi 712100, China
[c] Department of Biological Systems Engineering, Washington State University, Pullman, WA 99164-6120, USA

ARTICLE INFO

Article history:
Received 26 June 2015
Received in revised form
15 October 2015
Accepted 16 November 2015
Published online xxx

Keywords:
Modelling
Solar greenhouse
Temperatures
Evaluation method
Fuzzy set

Computer fluid dynamics (CFD) technique is considered as a powerful simulation tool to explore the temperature distribution in various buildings, especially for animal houses and greenhouses in recent years. However, its effective application in Chinese solar greenhouses (CSG) is still limited because of some technical problems and particular properties of CSG. A real-scale 2-D computer simulation model was developed with the finite-volume based commercial software, Fluent®, to simulate and analyse the temperature distributions caused only by thermal discharges from the north wall in CSG, governed by two computational domains, three conservation laws, and also five boundary conditions with k-ε turbulence model. A closed and empty CSG located in northwest of China was used to determine the thermal distribution and validate the simulation model during the night period on January 26th, 2013. Simulated and experimental results showed similar temperature distributions in CSG. The maximum and average absolute air temperature differences and mean squared deviation (MSD) were respectively 1.1, 0.8 and 0.1 K comparing measurement and simulation of inside air temperature and 0.7, 0.2 and 0.7 K for interior wall surface temperature. The simulation results demonstrated that temperature stratification and non-uniformity were more obvious when the north wall was thinner, suggesting a desirable thickness of north wall for energy conservation. The expanded polystyrene boards (EPS) play a more important role in preventing heat loss compared with perforated bricks (PB) in CSG. When the material cost was taken into consideration, a comprehensive evaluation model based on weighted entropy and fuzzy optimisation methods was employed to achieve the best north wall thickness (480 mm PB with 100 or 150 mm EPS) in CSG. The simulation and evaluation models in this study could be applied to enhance the indoor temperature environment and to optimise the thickness of the north wall in CSG.

* *Corresponding author*. College of Mechanical and Electronic Engineering, Northwest A&F University, Yangling, Shaanxi 712100, China. Tel.: +86 29 87092319; fax: +86 29 87091737.
** *Corresponding author*. Tel./fax: +86 29 87082179.
E-mail addresses: zouzhirong2005@hotmail.com (Z. Zou), shaojinwang@nwsuaf.edu.cn (S. Wang).
http://dx.doi.org/10.1016/j.biosystemseng.2015.11.006

Nomenclature

Γ_φ	generalised diffusion coefficient ($m^2\ s^{-1}$)
b_{ij}	normalised characteristic value
C_p	heat capacity ($J\ kg^{-1}\ K^{-1}$)
D	vector quantity of the worst relative membership degree
F_{cn}	cloud cover factor
f_{ij}	incoming function
G	vector quantity of the optimal relative membership degree
H	vector quantity of entropy value
h_0	surface convective heat transfer coefficients ($W\ m^{-2}\ K^{-1}$)
k	thermal conductivity ($W\ m^{-1}\ K^{-1}$)
m	number of indicators
n	number of cases
q	absolute heat flux ($W\ m^{-2}$)
q_{ex}	absolute heat flux of exterior wall surface ($W\ m^{-2}$)
q_{in}	absolute heat flux of interior wall surface ($W\ m^{-2}$)
r_{ij}	characteristic value for the relative membership with indicator i and case j
S_φ	source term ($W\ m^{-3}$)
T	temperature (K)
t	time (s)
T_a	average wall temperature (K)
T_{out}	outside air temperature (K)
T_{sky}	radiant sky temperature (K)
T_{soil}	soil surface temperature (K)
U	vector quantity of relative membership
u	velocity in the direction of x ($m\ s^{-1}$)
$\overline{v}$	velocity vector ($m\ s^{-1}$)
v	velocity in the direction of y ($m\ s^{-1}$)
V	surface real wind velocity ($m\ s^{-1}$)
v_1	wind velocity outside the CSG ($m\ s^{-1}$)
W_e	vector quantity of weight entropy
w	velocity in the direction of z ($m\ s^{-1}$)
x_{ij}	characteristic value for indicator i and case j
x_{imax}	maximum characteristic value of indicator i
x_{imin}	minimum characteristic value of indicator i
ρ	density ($kg\ m^{-3}$)

Subscripts

a	average
ex	exterior
in	interior
out	outside
P	monitored position
φ	universal variable

1. Introduction

Chinese solar greenhouses (CSG) are predominantly used in Chinese Mainland. The first group of CSG was initially developed since 1970s in Northeast China (Kang, 1990). In 2004, CSG reached 80% and 46% of the total area of protected cropping structures in Chinese Mainland and Northern China, respectively (Chen, 2008). The area of CSG has increased rapidly from less than 1100 ha in 1982 to more than 783,400 ha in 2010 (Wei et al., 2010). The value of CSG plant production reached more than US$115.1 billion in 2008, making a major contribution to economic growth of China (Guo et al., 2012). Therefore, it is desirable to study the microclimate in CSG to improve the plant growth environment (Tong, Christopher, Li, & Wang, 2013).

During winter, the lowest night ambient temperature can be below −20 °C in some northeast areas of China. Generally, the north wall in CSG is made of the material with a relatively high thermal storage coefficient to passively store a large quantity of heat during the day and then release the thermal energy during the night (Wang et al., 2010; Yang, 2012). Hence, a well-designed north wall in CSG can provide a desired thermal environment for plant growth. Single walls have been gradually replaced by layered walls because of better thermal insulation properties. Layered walls are commonly composed of two layers, such as perforated bricks (PB) and expanded polystyrene boards (EPS) (Fang & Gao, 2004; Li, Li, & Wen, 2009). PB may contribute more to thermal environment and hold more heat than sintered and clay bricks due to its perforated structure (Lacarrière, Trombe, & Monchoux, 2006). EPS as heat insulation materials have been widely used in buildings for many years (Demirel, 2013). Since costs of PB and EPS are much higher than those of other brick materials, it is important to determine a cost-effective thickness of the PB-EPS combined wall to meet the requirements for plant growth in CSG.

Computational fluid dynamics (CFD) has been proved to serve as an effective simulation tool to predict and analyse microclimate in animal buildings and greenhouses with the reliable results and low costs (Lee et al., 2013; Norton, Sun, Grant, Fallon, & Dodd, 2007). Most microclimate parameters in buildings, such as temperatures and airflow patterns, are strongly affected by the outdoor environment and properties of the related wall and covering materials, which can be simulated and predicted using CFD (Lee et al., 2013; Zerihun Desta et al., 2004). Animal buildings, such as broiler houses (Lee, Sase, & Sung, 2007) and pig houses (Seo et al., 2012), have been studied by using 3-D models in many cases in order to enhance the livestock productivity, maintain a comfort thermal environment and avoid undesired climate conditions. By using 3-D CFD models, airflow patterns and temperature distributions have been determined to explore the detailed convective heat transfer, the basic demands of vegetable growth (Boulard & Wang, 2002) and better greenhouse design (Boulard, Kittas, Roy, & Wang, 2002), and thermal and water vapour transfer as influenced by insect screening installed in the openings of greenhouses (Fatnassi, Boulard, Poncet, & Chave, 2006). The real-scale 3-D models have been widely used to simulate the microclimate distribution in greenhouses by incorporating solar radiation and latent or sensible heat exchange sub-models (Majdoubi, Boulard, Fatnassi, & Bouirden, 2009). However, the 3-D CFD models are too complicated to obtain accurate results in a short simulation time, resulting in increased interest in using the simple 2-D models. An early 2-D model of greenhouses

was applied to explore the temperature and airflow distributions (Mistriotis, Arcidiacono, Picuno, Bot, & Scarascia-Mugnozza, 1997). Similar 2-D models have also been used to determine greenhouse microclimate heterogeneity as influenced by covering materials (Muñoz, Montero, Anton, & Iglesias, 2004) and ventilation configurations (Bartzanas, Boulard, & Kittas, 2004). However, the development of temperature simulation model for CSG is relatively limited because of its particular properties, such as the changing covering material properties with time of day and season of the year (Tong et al., 2013). Some practical construction limitations also hinder research progress, such as the standard size and shape of the CSG, and ventilation or thermal preservation technology in different areas (Qi, 2005). The temperature distributions in CSG have been initially and tentatively studied using 2-D CFD models since the length of CSG is more than eight times that of the span (Tong, Li, Christopher, & Yamaguchi, 2007). Because north walls play an important role in CSG, relevant CFD studies have mainly focused on optimising their thickness (Tong, Christopher, Zhao, Wang, & Zhang, 2014) and structure (Wang et al., 2014). The 2-D CFD model can be an effective method to simulate the temperature distribution in CSG and optimise the thickness of the north wall.

The concept of entropy has been commonly introduced to evaluate all the data from simulation models. Entropy is defined as an academic concept referred to thermodynamics and characterised respectively both by the objective probabilities and some qualitative weights, objective or subjective (Guiaşu, 1971). Entropy weight is a statistical concept to depict the degree of disordered data, which could quantify uncertain problems on the weights (Ji, Huang, & Sun, 2015). Therefore, the entropy method can be described as an approach, in which the weight values of individual indicators are determined by computing the entropy and entropy weight (Lin, Wen, & Zhou, 2009; Qi, Wen, Wang, Li, & Singh, 2010). This notion was primarily defined by the base of Shannon's function (De Luca & Termini, 1972; Jin, Pei, Chen, & Zhou, 2014). A series of entropy weights, composing a fuzzy set in which elements have a single value between zero and one according to its own membership degree in the set, was first introduced by Zadeh (1968). Theoretically, the larger the differences of indices, the more important the variables are in weighted entropy method, and the larger weight may be assigned. The fuzzy optimisation method has been adopted to choose the generated optimal weighted entropies according to the maximum entropy principle (Bierkens & Kappen, 2014; Jin et al., 2014; Wu & Zhang, 2011). This methodology aims at correctly selecting optimal options by ignoring personal preferences in multivariable systems (Teferra, Shields, Hapij, & Daddazio, 2014) and has been accepted broadly in some research fields, including hydraulic engineering, agricultural irrigation fields and computer vision applications (Zhou, Zhang, & Wang, 2007). This methodology has been validated to effectively solve the problem of low-efficiency, subjectivity, and one-sidedness. The greenhouse environment has many variables interacted with each other, such as temperature, humidity, heat flux, and investment etc. Thus, the introduction of weighted entropy and fuzzy optimisation methods has the potential to achieve a better selection of north wall thickness in CSG.

The objectives of this study were 1) to explore the thermal environment in CSG using CFD unsteady simulations, 2) to validate the CFD model by comparing with the measured data, 3) to predict the different thermal environments with varying thicknesses of combined north walls, and 4) to optimise the north wall based on its thickness and cost using weighted entropy and fuzzy optimisation methods.

2. Materials and methods

2.1. Experimental CSG

The experimental CSG (Fig. 1) was located in the Innovative Base of Modern Agriculture High-technology Industrial District, Yangling (latitude: 34°2′ N, longitude: 108°4′ E, altitude: 499 m), Shaanxi, China where the average annual air temperature and precipitation in 2013 were 14.6 °C and 481.1 mm, respectively, provided by Yangling Meteorological Station. The PB-EPS combined north wall of experimental CSG was 3.3 m high and 0.72 m thick (th) with the PB and EPS thicknesses of 360 and 300 mm, and the angle of back roof was 45°. The back roof was made of magnesia cement 71 mm thick and the width of the thermal insulating covering (quilt, the blue material shown in Fig. 1a mostly composed of felts, cottons, and non-woven tissues etc. with relevant thermo-physical properties in Table 1) was 12 mm (Fig. 2). It was regularly covered with the quilt at 5:00 p.m. and uncovered at 8:30 a.m. the following morning during winter. The night sky was clear and the CSG was empty during the whole experimental period.

2.2. Computer simulation

2.2.1. Physical model

A real-scale 2-D model (Fig. 3) of experimental CSG was created and composed of two modules for the fluid computational domain, such as the inside and outside air, and the solid computational domains, including quilt, back roof, EPS, PB, and soil. Energy and Standard $k-\varepsilon$ Turbulence Models were selected.

2.2.2. Model simplifications

1) Since the inside air of CSG was regarded as an airtight region at night, no humidity sink or source was taken into consideration.
2) The air exchange between inside and outside of CSG was neglected since natural ventilation was negligible for closed CSG.
3) Influences of humidity and heat from plants were not taken into consideration since the CSG was empty during the experiment.
4) For further simplifying this model, the latent heat exchange between soil and the surrounding air was also neglected since their water content was low and the heat flux from the soil was much smaller than that to the north wall.

Fig. 1 – The overall appearance (a) and internal layout (b) of experimental Chinese Solar Greenhouse (CSG) located in Yangling, Shaanxi, China with dimensions 80 m long (E–W) and 10 m wide (S–N).

Table 1 – Thermo-physical properties of materials used for computer simulation.

Material	ρ (kg m^{-3})	C_p (J kg^{-1} K^{-1})	k (W m^{-1} K^{-1})	Viscosity (kg m^{-1} s^{-1})	Thermal expansion coefficient (K^{-1})
Inside air	1.205	1013	0.027	1.81×10^{-5}	0.003466
Perforated brick (PB)	1400	750	0.580	–	–
Expanded polystyrene board (EPS)	38	1300	0.047	–	–
Quilt	70	1677	0.040	–	–
Magnesia cement	1700	800	0.500	–	–

2.2.3. *Governing equations*

CFD is a numerical methodology for solving the governing equations of fluid flow using finite volume method to convert the partial differential equations to a set of algebraic equations (Molina-Aiz, Fatnassi, Boulard, Roy, & Valera, 2010). It is based on the resolution of governing equations of three conservation laws, which include the momentum, energy, and mass transport equations as follows (Versteeg & Malalasekera, 1995):

$$\frac{\partial(\rho\varphi)}{\partial t} + div(\rho\varphi\overline{v}) = div(\Gamma_{\varphi} grad\varphi) + S\varphi \quad (1)$$

where φ is the universal variable; ρ, $\overline{v}$, Γ_{φ}, and S_{φ} are the density (kg m^{-3}), velocity vector (m s^{-1}), generalised diffusion coefficient (m^2 s^{-1}), and source term (W m^{-3}), respectively. It is a continuity equation when φ is 1, an energy equation when φ is T (K) and a momentum equation when φ is u, v, w (m s^{-1}), the velocities in the directions of x, y, and z, respectively.

2.2.4. *Initial and boundary conditions*

Five types of boundary conditions were defined, for outside air temperature (T_{out}), radiant sky temperature (T_{sky}), surface convective heat transfer coefficients (h_0) under different wind

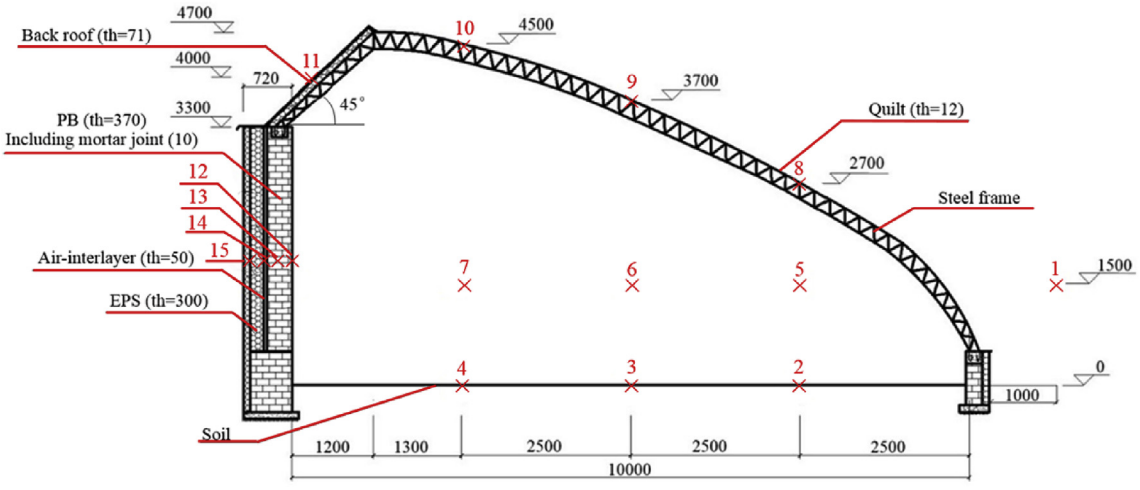

Fig. 2 – Materials and dimensions (th) of experimental Chinese Solar Greenhouse (CSG) in cross-section. Combined north wall consisted of perforated brick (PB), air-interlayer, and expanded polystyrene board (EPS) from inside to outside. Specifically monitored positions (P1–P15) were used for collecting the experimental data (all dimensions are in mm).

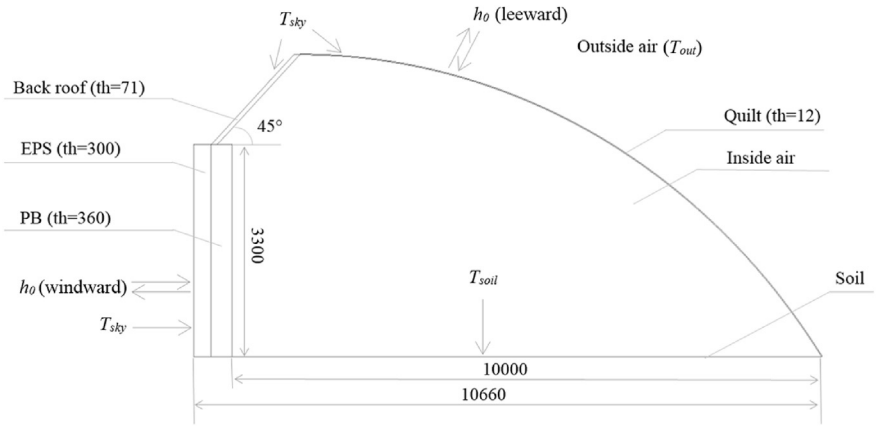

Fig. 3 – 2-D diagram and dimensions (th) of the experimental Chinese Solar Greenhouse (CSG) used in simulation (all dimensions are in mm).

directions, and soil surface temperature (T_{soil}). The initial temperature of the outside air was set as 288.2 K, the average air temperature during the experimental period. The model was first run under steady state conditions, and the results were used to launch the unsteady simulations. The air temperature at night changed with time and only the conduction equation (conjugate heat transfer) was solved inside the walls, which can be fitted based on the experimental data during 18:30 (t = 0 s) to 8:10 (t = 49,200 s) on the following morning as follows:

$$T_{out} = \left(-1.532 \times 10^{-13}\right)t^3 + \left(1.573 \times 10^{-8}\right)t^2 - \left(6.674 \times 10^{-4}\right)t + 283.5 \quad (2)$$

where T_{out} is the outside air temperature (K); t is the time (s), $0 \le t \le 49{,}200$. Rate of heat transfer between the exterior wall surface of CSG and outside air can be determined by the convective heat transfer coefficient, which can be calculated by Eqs. (3)–(5) when the wind speed is known (Mirsadeghi, Cóstola, Blocken, & Hensen, 2013):

$$h_0 = 18.63V^{0.605} \quad (3)$$

$$\text{Leeward}: \quad V = 0.3 + 0.05v_1 \quad (4)$$

$$\text{Windward}: V = \begin{cases} 0.25v_1, & v_1 \ge 2ms^{-1} \\ 0.50, & v_1 < 2ms^{-1} \end{cases} \quad (5)$$

where h_0 is the surface convective heat transfer coefficient (W m^{-2} K^{-1}); V is the surface real wind velocity (m s^{-1}); v_1 is the wind velocity outside the CSG (m s^{-1}).

The thermal radiant exchange with the sky influences the heat balances of the roof and the cladding material. It is therefore necessary to determine the radiant sky temperature T_{sky}. As the latter is highly dependent on the cloud cover, an empirical formula proposed by Swinbank (1963) was used:

$$T_{sky} = F_{cn}T_{out} + 0.0552(1 - F_{cn}){T_{out}}^{1.5} \quad (6)$$

where F_{cn} is the cloud cover factor (1 overcast and 0 clear). For example, $T_{sky} = 270.1$ K when the outside air temperature (T_{out}) is 288.2 K with clear sky ($F_{cn} = 0$).

For conveniently validating and utilising the established simulation model, soil was regarded as playing an inertial role, according to the last simplifying assumption, in CSG (Li, Bai, & Zhang, 2010) and therefore was not considered (this amounts to assuming that changes of north wall characteristics have little impact on soil part of heat exchange) and was not meshed in the simulation model. More studies of soil (radiation and convection heat transfer) can be found in the work of Abdel-Ghany and Kozai (2006). Soil surface temperature (T_{soil}, K) was also fitted by quadratic function based on the real-time experimental data as follows:

$$T_{soil} = \left(1.366 \times 10^{-9}\right)t^2 - \left(2.316 \times 10^{-4}\right)t + 294.8 \quad (7)$$

2.2.5. *Solving methodology*

Fluent® software (ANSYS 14.5, ANSYS Inc. Lebanon, NH, USA) was used to simulate the temperature distributions in the CSG at night. The software was run on a Dell computer with Quad-Core 3.40 GHz Intel Processors, 8 GB RAM on a Windows 7 64 bit operating system. Figure 4 illustrates the steps taken in the simulation. With the consideration of volume influence of each part, some refinements were made in the quilt (1500 computational cells in 12 mm width) and PB-EPS combined north wall (12,211 computational cells in 300 or 360 mm width) to guarantee the accuracy of temperature distribution results. Other parts of the computational domain were meshed with normal sizes. The total number of 26,835 computational cells was generated by using the mesh function to divide the model (compared and validated in the 3.2. section). Quality of grid was primarily checked and entirely satisfied by the skewness (0.05) and orthogonal parameters (0.99) (ANSYS, 2011). Since the thermal boundary conditions changed gradually and smoothly during night, it was tried conventionally to reduce time step each time instead of increasing in the value for iteration per time step when the convergence issue appeared. The number of time steps and time step size eventually used in this study therefore were set as 820 and 60 s (t = 49,200 s), respectively, with 20 iterations per time step in the simulation. Transient state and pressure-based solver were adopted for the momentum, energy, and continuity equations. Turbulence was activated using the standard k-ε model with

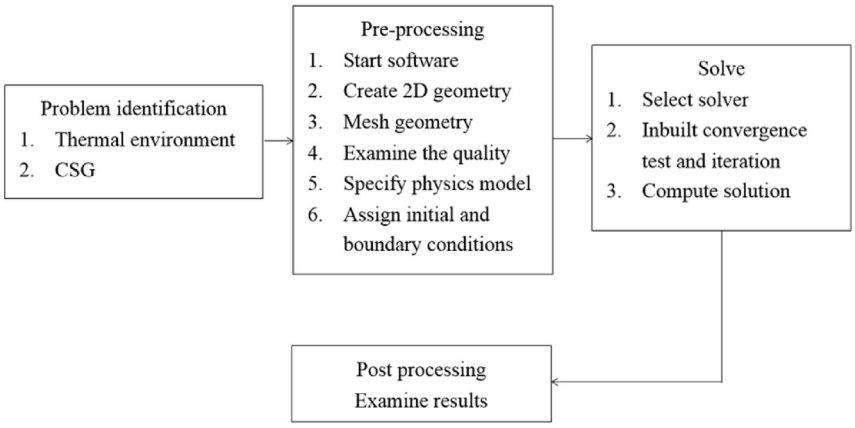

Fig. 4 – Flow chart of modelling steps using Fluent®.

standard wall functions. Second order upwind was chosen for the discretisation schemes and SIMPLEC method was used for coupled momentum of pressure and velocity. The convergence criteria of residuals were below 10^{-5} for energy equations and 10^{-3} for continuity and $k - \varepsilon$ equations. Each simulation task took around 40 min.

2.2.6. *Model parameters*

The material density was determined by the volume method based on mass. The thermal properties (C_p and k) of PB, EPS, quilt, and magnesia cement were measured using thermal storage apparatus (XRY-II, Xiangtan City Instrument & Meter Co., LTD, Xiangtan, China) at room temperature and humidity. The thermo-physical properties of materials under greenhouse temperatures are listed in Table 1 for computer simulation, where the thermal expansion coefficient (K^{-1}) of air was also provided since the air density (ρ) was highly influenced by environmental temperature.

2.3. *Experimental procedure and model validation*

Figure 2 shows the main cross-section of CSG supported by the steel frame. Days on January 25th and 26th, 2013, with a clear night, were chosen for the measured data. Complementary research for the diurnal period can be found elsewhere (Tong, Christopher, & Li, 2009). Wind velocity and direction were 0.2 m s^{-1} and north by northwest for this night period. No ventilation openings were available in the CSG to modify night temperatures. By calculation, value of h_0 at the front roof was 9.17 W m^{-2} K^{-1} when considered as leeward; and value of h_0 at the north wall was 12.25 W m^{-2} K^{-1} when considered as windward. The monitored positions (P1–P16, Table 2) were in the central cross-section of CSG span, Fig. 2. Air and soil surface temperatures (P1–P7) were recorded using long-term data loggers (PDE-R10, Wuge Technology of Electronics Co., Ltd, Harbin, China), using air temperature and soil surface temperature sensors (platinum resistance thermometer, PT 100, valid temperature range of −40 °C to 120 °C, with precision of ±0.5 °C). Quilt and back roof surfaces (P8–P12), and inner temperatures of north wall (P13–P15) were recorded by multi-sensor temperature data loggers (HL-2008, Haolong Electromechanical Device Co., Ltd, Hangzhou, China) with the valid temperature range of −50 °C to 300 °C, and the precision of ±0.5 °C. Measurements were made every second, and averaged and consecutively stored as data every 10 min. The recording period was set for a week (from January 22nd to 28th). Figure 5 shows the full data set of temperatures (P1, P3, P6 and P12), illumination conditions (P1 and P6, recorded by illumination sensor with the valid range of 0–200,000 lux and precision of ±5%) inside and outside the CSG, and relative humidity (RH, P3 and P6, recorded by RH sensor with the valid range of 0–99% and precision of ±3%) during the whole experimental week with clear days and nights, which reasonably supported the first and the third simplifications made in Section 2.2.2. The simulated results were compared with the measured data to validate the computer model.

2.4. *Model applications*

Once the computer simulation was validated, it could be used to predict the performance of heat retention in terms of varying thicknesses of north wall, as listed in Table 3. Same model parameters, initial and boundary conditions and solving methodology were used in the models.

2.5. *Comprehensive evaluation*

2.5.1. *Structure of evaluation model*

Structure of comprehensive evaluation model is shown in Table 4. Similar evaluation models can also be found elsewhere (Jin et al., 2014; Jing, Ng, & Huang, 2007; Li & Hu, 2006; Qi et al., 2010; Zhou et al., 2007). Three main aspects, which can be representative for the performance of north wall in CSG, have been selected to establish the comprehensive evaluation model for further calculation, including temperatures, absolute heat fluxes in Fig. 6 and the construction cost (*CC*) in Table 5. All of the simulated data except for *CC* were obtained from the model outputs and post processing. *CC* was derived from the local construction market in 2013 in Shaanxi Province, China (Table 5).

Table 2 – Measurement details of specifically monitored positions (P1–P16) at the cross-section shown in Fig. 2.

Monitored position (P)	Measured items	Monitored position (P)	Measured items
1	Air temperature	9	Quilt temperature
2	Soil surface temperature	10	Quilt temperature
3	Soil surface temperature	11	Back roof temperature
4	Soil surface temperature	12	Interior surface temperature
5	Air temperature	13	Mid-PB temperature
6	Air temperature	14	Air-interlayer temperature
7	Air temperature	15	Mid-EPS temperature
8	Quilt temperature	16 (Not shown)	Wind velocity (open space)

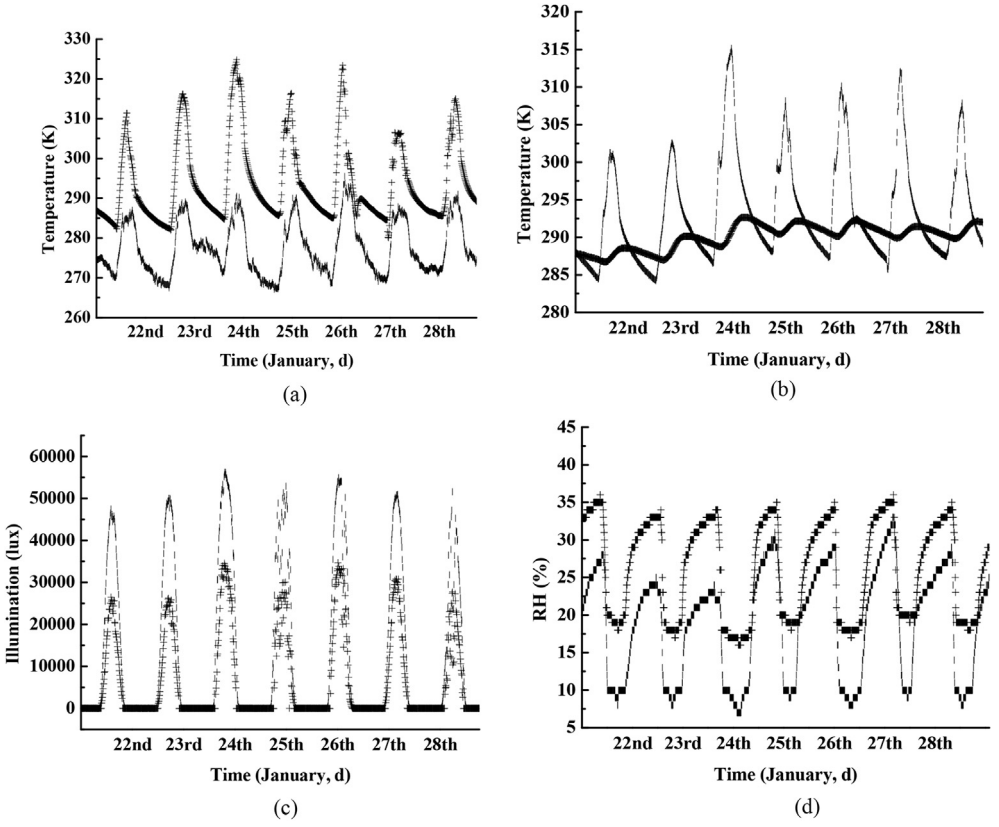

Fig. 5 – Temperatures (K) at P1 (|) and P6 (+) (a), P3 (+) and P12 (|) (b), illumination conditions (lux) at P1 (|) and P6 (+) (c) inside and outside Chinese solar greenhouse (CSG), and relative humidity (RH, %) at P3 (+) and P6 (|) (d) during a whole experimental week, from January 22nd to 28th, 2013.

Table 3 – 18 cases of combined perforated brick-expanded polystyrene board (PB-EPS) north wall thickness for simulation.

Case	PB-EPS thickness (mm)	Case	PB-EPS thickness (mm)
1	240–50	10	240–200
2	360–50	11	360–200
3	480–50	12	480–200
4	240–100	13	240–250
5	360–100	14	360–250
6	480–100	15	480–250
7	240–150	16	240–300
8	360–150	17 (Case validation)	360–300
9	480–150	18	480–300

2.5.2. *Establishment of evaluation model*

1) A set of cases and objectives were built for decision-making problems of multi-objectives. The decision-making characteristic matrix is composed of objective values and can be transformed into an indicative degree of membership matrix, with evaluating indicators. The process of transformation depends on the efficiency type (the larger is better, including T and q_{in}) or the cost type (the smaller is better, including q_{ex} and CC).
2) Optimal matrix with fuzzy partition can be established by extracting the maximum and the minimum value in each row of the indicative degree of membership matrix.
3) To establish the objective function, the weight vector of evaluating indicators should be determined. Then the

Table 4 – Structure of comprehensive evaluation model for further calculation of weighted entropy and fuzzy optimisation methods. The specific positions in the 3rd hierarchy are illustrated in Fig. 6.

The 1st hierarchy	The 2nd hierarchy	The 3rd hierarchy
Comprehensive evaluation model of north wall in CSG	Temperature (T)	Inside air temperature (T_{P6})
		Interior wall surface temperature (T_{P12})
		Average wall temperature (T_a)
	Absolute heat flux (q)	Absolute heat flux of interior wall surface (q_{in})
		Absolute heat flux of exterior wall surface (q_{ex})
	Construction cost (CC)	Construction cost (CC)

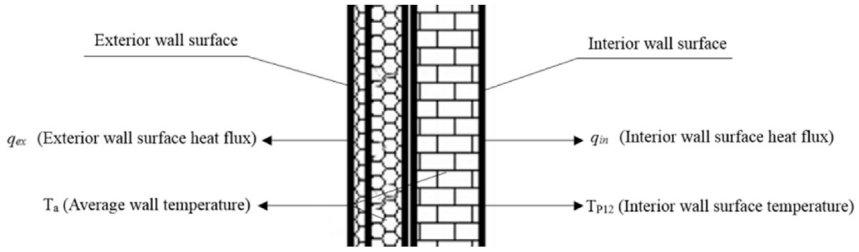

Fig. 6 – Four selected characteristic parameters in the optimised model. T_{P12} and T_{P6} are the temperatures measured at positions of P12 and P6 in Fig. 2.

optimal value of relative membership degree of all the cases may be deduced, in terms of the criterion of the minimum summation of quadratic optimal and quadratic worst weighted Euclidean distances.

4) Comprehensive evaluation model of thermal insulation properties can be finally received by differentiating the objective function and assigning zero value to that derivative. Weight vector of evaluating indicators can be determined by employing weighted entropy method, calculating the degree of memberships with different cases and then ordering them by using fuzzy optimisation. According to the maximum entropy principle, the case would be theoretically considered as optimal its membership was larger than the others.

2.5.3. *Characteristic values in the model*

According to the structure of the comprehensive evaluation model in Table 4, six characteristic values were carefully chosen from the results of modelling, which were partly shown in Fig. 6 and fully listed in Table 5. The *CC* consists of unit cost of PB (US$15.81 per 240 mm^{-1} and m^{-2}), that of EPS (US$18.25 per 50 mm^{-1} and m^{-2}) and labour cost.

2.5.4. *Optimisation and calculation procedure*

1) If n (n = 18 in this paper) was defined as the number of cases satisfying the constraint conditions, m (m = 6 in this paper) was defined as the number of indicators to distinguish between advantages and disadvantages with

Table 5 – Characteristic values of selected 6 indicators in 18 cases for optimising models.

Case	T_{P6} (K)	T_{P12} (K)	T_a (K)	q_{in} (W m^{-2})	q_{ex} (W m^{-2})	Construction cost (CC, US$ mm^{-1} m^{-2})
1	282.6	285.1	283.8	49.40	36.61	68.13
2	283.0	286.3	285.9	75.14	42.74	83.94
3	283.3	287.0	287.4	87.29	45.86	99.75
4	283.8	286.6	284.8	61.32	18.33	104.64
5	284.1	287.6	286.8	81.23	21.38	120.45
6	284.5	288.4	288.6	95.17	22.94	136.26
7	284.0	287.0	284.5	67.38	10.43	141.15
8	284.3	288.1	286.8	90.07	13.52	156.96
9	284.7	288.7	288.5	99.48	13.63	172.77
10	284.5	287.8	285.3	75.19	3.95	177.65
11	284.8	288.6	287.0	88.49	9.14	193.46
12	285.2	289.3	288.8	100.77	9.93	209.27
13	284.7	287.9	284.9	71.84	5.79	214.16
14	285.1	288.9	287.1	92.79	8.08	229.97
15	285.4	289.5	288.7	101.37	7.69	245.78
16	284.8	288.0	285.0	73.27	6.04	250.67
17	285.9	289.6	287.4	91.32	7.11	266.48
18	286.1	289.6	289.4	102.43	7.55	282.29

evaluating objective, the decision-making characteristic matrix **X**, with n cases and m indicators, could be obtained as follows:

$$\mathbf{X} = (x_{ij}) \tag{8}$$

where x_{ij} is the characteristic value for indicator i and case j, $i = 1, 2, \ldots, m$; $j = 1, 2, \ldots, n$. All the values in matrix **X** are given in Table 5.

2) Generally, evaluating indicators of comprehensive performance with north wall can be divided into the efficiency and cost types when optimising. To calculate the relative membership, computational equations for these two types of indicators are:

$$r_{ij} = (x_{ij} - x_{i\ min})/(x_{i\ max} - x_{i\ min}) \quad \text{for efficiency type} \tag{9}$$

$$r_{ij} = (x_{i\ max} - x_{ij})/(x_{i\ max} - x_{i\ min}) \quad \text{for cost type} \tag{10}$$

where x_{imax} is the maximum characteristic value of indicator i; x_{imin} is the minimum characteristic value of indicator i.

Decision-making characteristic matrix **X** can be transformed into an indicative degree of membership matrix **R** according to Eqs. (9) and (10):

$$\mathbf{R} = (r_{ij}) \tag{11}$$

where r_{ij} is the characteristic value for the relative membership with indicator i and case j.

The indicative degree of membership matrix **B** can be got after normalising matrix **R**:

$$\mathbf{B} = (b_{ij}) \tag{12}$$

where b_{ij} is the normalised characteristic value.

The optimal relative membership degree **G** and the worst relative membership degree **D** within n cases can be defined as follows:

Table 6 – Indicative membership matrix R and normalised matrix B ($i = 1, 2, \ldots, m$; $j = 1, 2, \ldots, n$).

	Matrix R (Matrix B) i					
	0.000	0.000	0.000	0.000	0.221	1.000
	0.105	0.259	0.382	0.485	0.074	0.926
	0.199	0.417	0.648	0.715	0.000	0.852
	0.322	0.330	0.181	0.225	0.657	0.830
	0.419	0.548	0.542	0.600	0.584	0.756
	0.519	0.718	0.864	0.863	0.547	0.682
	0.379	0.419	0.136	0.339	0.845	0.659
	0.479	0.650	0.549	0.767	0.772	0.585
j	0.578	0.785	0.842	0.944	0.769	0.511
	0.527	0.585	0.273	0.486	1.000	0.489
	0.627	0.763	0.571	0.737	0.876	0.415
	0.724	0.916	0.908	0.969	0.857	0.341
	0.590	0.614	0.197	0.423	0.956	0.318
	0.695	0.843	0.598	0.818	0.901	0.244
	0.786	0.971	0.890	0.980	0.911	0.170
	0.618	0.643	0.214	0.450	0.950	0.148
	0.940	0.998	0.655	0.790	0.925	0.074
	1.000	1.000	1.000	1.000	0.914	0.000

$$\mathbf{G} = (g_1, g_2, \cdots, g_m)^{\mathrm{T}} \tag{13}$$

$$\mathbf{D} = (d_1, d_2, \cdots, d_m)^{\mathrm{T}} \tag{14}$$

where $g_i = \vee_{j=1}^{n} r_{ij}$ and $d_i = \wedge_{j=1}^{n} r_{ij}$. The symbols used here ($\vee$, $\wedge$) mean that the extreme values (maximum value, minimum value) are expected to be chosen through the definitions (Qi et al., 2010; Qin, 2003; Zhou et al., 2007).

Indicative membership matrix **R** and normalised matrix **B** can be acquired by Eqs. (9) and (10), as presented in Table 6.

B is same as **R** because of the Eqs. (13) and (14) are as follows:

$$\mathbf{G} = (1,\ 1,\ 1,\ 1,\ 1,\ 1)^{\mathrm{T}} \text{ and } \mathbf{D} = (0,\ 0,\ 0,\ 0,\ 0,\ 0)^{\mathrm{T}}$$

3) Entropy value H_i can be determined as follows:

$$H_i = -\frac{1}{\ln n}\left[\sum_{j=1}^{n} f_{ij} \ln f_{ij}\right] \tag{15}$$

$$f_{ij} = \frac{b_{ij}}{\sum_{t=1}^{n} b_{it}} \tag{16}$$

where $0 \le H_i \le 1$, f_{ij} is an incoming function, $f_{ij} \ln f_{ij} = 0$ was assumed to validate $\ln f_{ij}$ when $f_{ij} = 0$, $i = 1, 2, \ldots, m$; $j = 1, 2, \ldots, n$.

Therefore, vector quantity of entropy value **H** can be computed by Eqs. (15) and (16):

$$\mathbf{H} = (0.948,\ 0.960,\ 0.933,\ 0.958,\ 0.953,\ 0.927)^{\mathrm{T}}$$

Obviously, the average entropy values of evaluation model is 94.7%, which may possibly explain the reason that all of the indicators can represent the majority of original information (Zhang, Zhang, & Chi, 2010).

Weight entropy of evaluating indicator W_{ei} can be calculated as follows:

$$w_{ei} = \frac{1 - H_i}{m - \sum_{i=1}^{m} H_i} \tag{17}$$

where $i = 1, 2, \ldots, m$. Therefore, vector quantity of weighted entropy W_e can be computed by Eq. (17):

$$\boldsymbol{w}_e = (0.162,\ 0.125,\ 0.208,\ 0.131,\ 0.146,\ 0.228)^{\mathrm{T}}$$

4) Membership u_j of case j can be achieved by adopting weighted and generalised Euclidean distance method and the least square method:

$$u_j = \left\{1 + \frac{\sum_{i=1}^{m}\left[w_{ei}(g_i - r_{ij})\right]^2}{\sum_{i=1}^{m}\left[w_{ei}(r_{ij} - d_i)\right]^2}\right\} \tag{18}$$

Therefore, vector quantity of relative membership degree **U** with 18 cases can be achieved by Eq. (18). This relative degree of membership was compared for the 18 cases listed in

Table 5 and used to guide the optimal selection of the designed north wall.

3. Results and discussions

3.1. Simulated temperature and airflow patterns in experimental CSG

As shown in Fig. 7a, simulated temperatures in experimental CSG revealed that PB and soil had the higher temperatures, while the EPS, back roof, and the exterior front roof surface had the low temperatures, which are in good agreement with previous reports (Tong & Christopher, 2009; Tong et al., 2009). They also found that the temperatures in vicinity of the inner surface of the front roof during the night could be lower than the air temperatures even when covered with the thermal insulating material, suggesting that thermal loss frequently occurs via the surfaces that are more exposed to the outside environment. Inside air temperature was between the cold surface and warm surface temperatures due to heat convection. There was also a clear temperature gradient between PB and EPS in the north wall (Wang et al., 2014). Figure 7b shows a clear clockwise airflow around the internal walls of the CSG. The highest air speed of 1.22 m s^{-1} was found near the north wall where the large temperature difference may mainly result in the swirling flow of inside air. Majdoubi et al. (2009) found that buoyancy forces, mostly triggered by air temperature increases, actually lead to air loops between the greenhouse roof and crop canopy, and this can even occur in an empty greenhouse (Mistriotis et al., 1997; Sase, Takakura, & Nara, 1983). Similar findings have been reported by Lamrani (1997) and Boulard, Lamrani, Roy, Jaffrin, and Bouirden (1998), where though the air movement was only induced by the temperature difference between soil and roof, the measured air speed had the same order of magnitude as in natural ventilation. The stable airflow with a low speed was observed in the centre of the CSG. Similar airflow patterns in greenhouses have been reported elsewhere (Mistriotis et al., 1997; Wang, Luo, & Li, 2013).

3.2. Model validation

The simulated temperature at each measurement position (Tong et al., 2009) was in good agreement with the experimental one with a same decreasing trend over the measurement period (Fig. 8). For example, the maximum and average absolute temperature differences between measurement and simulation were 1.1 K and 0.8 K, respectively, at P6. These values became 0.7 K and 0.2 K at P12. The different D-values between maximum and minimum temperatures (T_{sky} and T_{soil}) used as boundary conditions in the domain are respectively 13.0 and 8.1 K. Figure 8a showed a relatively large discrepancy between experiment and simulation for P12 temperature trend whereas Fig. 8c showed a much smaller discrepancy for the average of P12–P15. This implied that the gradient of temperature over this distance may be much less in the model than in measurements. Mean squared deviation (MSD) of simulated and measured data at monitored positions (P2–P15) are shown in Fig. 9. The lower the value of MSD, the closer the simulation was to the measurement (Kobayashi & Salam, 2000). In addition, the MSD is 0.07 K between the two simulated results at P6 in 26,835 and in 54,741 computational cells (improved mesh) individually, which reasonably supports the quality of current mesh. The precision of this CFD model was validated against experimental data, and it may serve as a useful tool to predict the effect of heat preservation and temperature distributions.

3.3. Model prediction

3.3.1. Temperature distributions

There is an obvious temperature increase from case 1 (Fig. 10a) to 18 (Fig. 10b) by comparing profiles. Some obvious thermal stratification was observed with inside air since the area in the immediate vicinity of the north wall had the higher temperature, whilst the area next to the front roof had the lowest. A drastic decrease of temperature was detected close to the cover (Muñoz et al., 2004; Tong et al., 2009; Wang et al., 2013).

Both the average temperature of inside air (T_{P6}) and interior wall surface (T_{P12}) and the heat flux of exterior (q_{ex}) and interior (q_{in}) wall were the best when the thicknesses of EPS and PB took their highest values, were 300 mm and 480 mm respectively (Fig. 11), and worst with the lowest values (Tong et al., 2014). The only exception was for the absolute value of q_{ex} of case 10 (Fig. 11a), which was relatively small (due to the low heat loss during night) when the thickness of EPS and PB were 200 mm and 240 mm respectively. Obviously, q_{ex} would be smaller and the heat loss might be less when the thicknesses of heat insulation materials of north wall were thicker

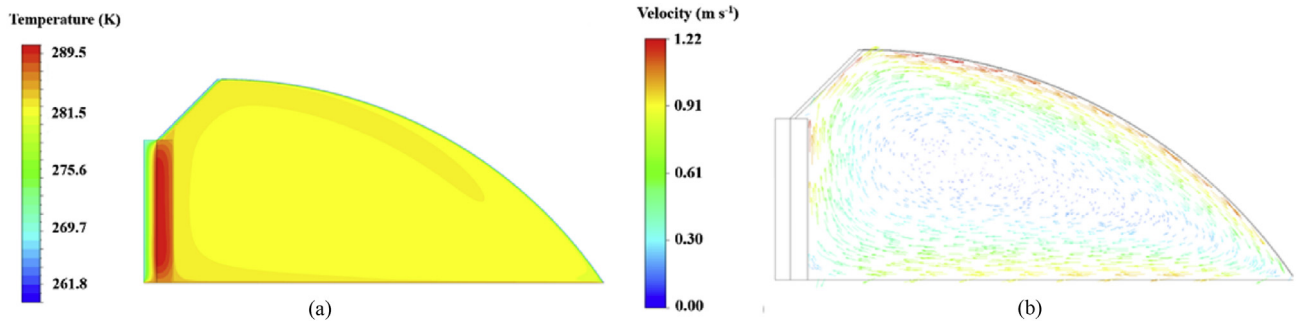

Fig. 7 – (a) Simulated temperature (K) and (b) wind velocity (m s^{-1}) distributions in the experimental Chinese Solar Greenhouse (CSG) at 8:10 on January 26th, 2013.

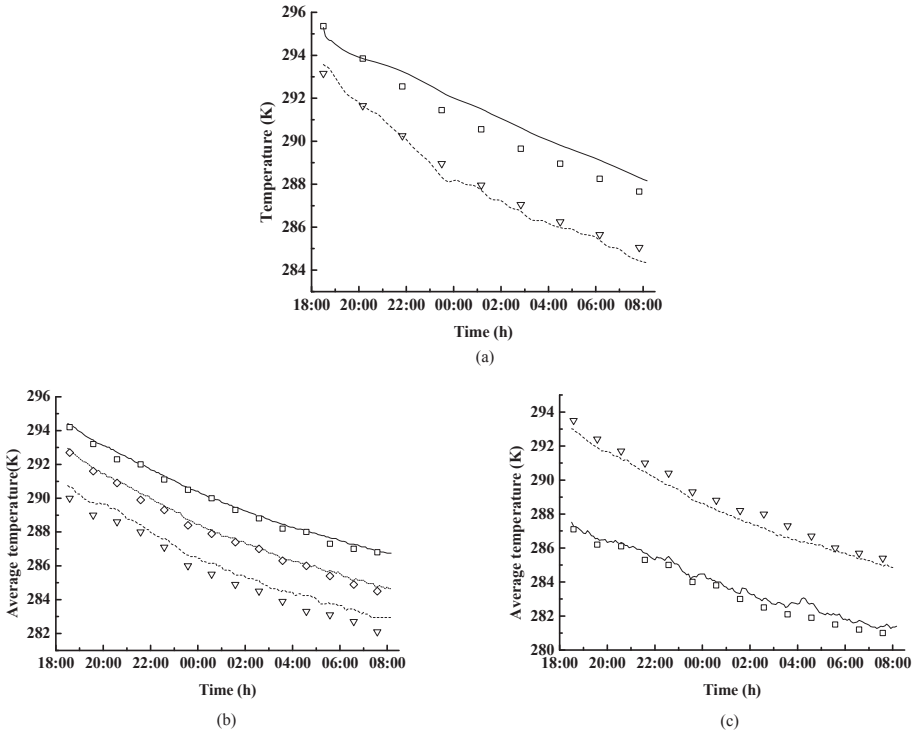

Fig. 8 – Experimental (symbols) and simulated (lines) temperature-time histories of monitored positions of P6 (▽, air temperature) and P12 (□, interior surface temperature of perforated brick (PB)) (a) and average temperature-time histories of monitored positions of P2–P4 (□, soil), P8–P10 (▽, quilt) and P11 (◇, back-roof) (b) and of P5–P7 (▽, inside air) and P12–P15 (□, north wall) (c) over the whole period from 18:30 on 25th to 8:10 on January 26th, 2013.

because of the final performance of thermal prevention was determined by the whole combination of wall cases. Thus, because of the less heat prevention (small sink) for this wall case during the day and the less heat loss (small source) from the wall to the outside space during the night, the heat flux performance of this wall would be better than for some of others. When the thicknesses of EPS and PB were decreasing at the same time, the changes of both temperature and heat flux were non-linear (Wang et al., 2014). This result suggests that there is a certain thickness of north wall in CSG that could meet the basic needs to grow the plant and be economically optimal by constraining the cost.

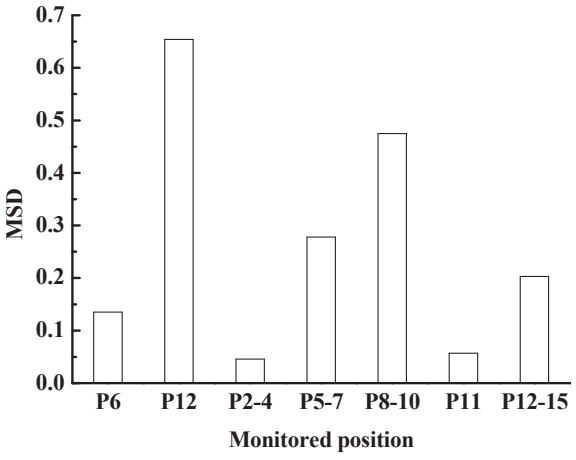

Fig. 9 – Mean squared deviation (MSD) in a comparison of simulated and measured temperatures at monitored positions of P2–P15 in experimental Chinese solar greenhouse (CSG).

According to simulation results during the day time, the radiation energy is generally transferred through the north wall, roof, and soil (Tong et al., 2009). Our study found that the north walls were constantly releasing the heat to the indoor air during night (Fig. 9a and b) because the T_{P12} was clearly higher than T_{P6} by around 3–4 K. These observations also can be reasonably supported by some experimental results (Li & Chen, 2006). All of the T_{P6} values using 50 mm thickness EPS were lower than 283.5 K (10 °C) before CSG was uncovered in the morning (Fig. 11a). Therefore, 100 mm thickness of EPS should be taken into consideration at least for growing thermophilic plants (Yang et al., 2009). Besides, EPS plays an important role in preventing heat loss because there is a dramatic temperature change when the thickness of EPS is increased while the PB remains the same thickness. However, this temperature trend was gradually weakened when the EPS thickness increased from 200 mm to 300 mm and if the thickness of PB was increased during this time, the temperature change was also significant. For example, there was a clear temperature change when the thickness of PB increased from 240 mm to 360 mm with the EPS thickness of 300 mm. The simulated T_{P12} followed the same change pattern as T_{P6} for all combinations, during the night (Fig. 11b).

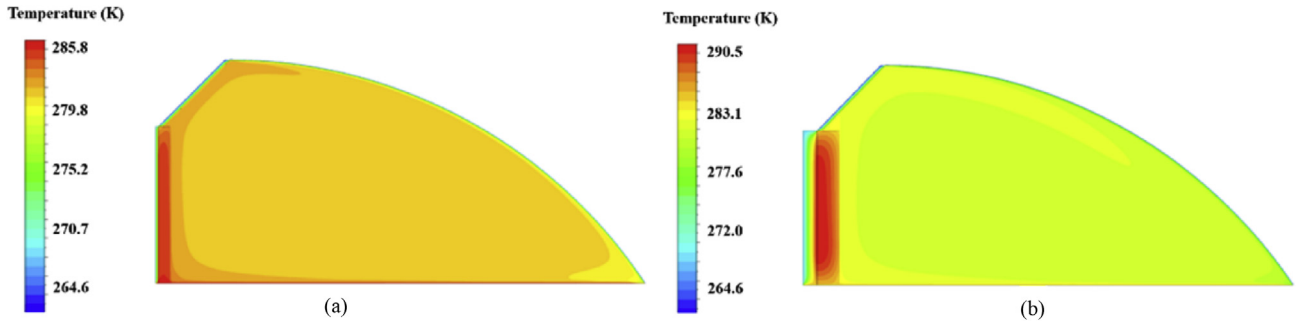

Fig. 10 – Simulated temperature profiles of (a) case 1 and (b) case 18 simulations of Chinese Solar Greenhouse (CSG), after 49,200 s transient simulation with the same initial and boundary conditions, from 18:30 on 25th to 8:10 on January 26th, 2013.

3.3.2. *Heat flux distributions*

D-value (becoming larger as the north wall became thicker) between q_{in} and q_{ex} in each simulated model can be clearly observed (Table 5), implying that the solar energy stored inside the north wall was continuously being released to the inside air rather than being lost to the outside during the whole night. The heat flux had a wider change between the lowest and the highest values (Fig. 11c and d). This could be caused by the first model simplification, in which the air leakage in the CSG was neglected by simply considering as an airtight space during the simulation time (Tong et al., 2013). The heat flux profiles were significantly affected by the thickness of EPS rather than PB (Fig. 11c). For example, when the thickness of PB remained as 480 mm, the heat flux

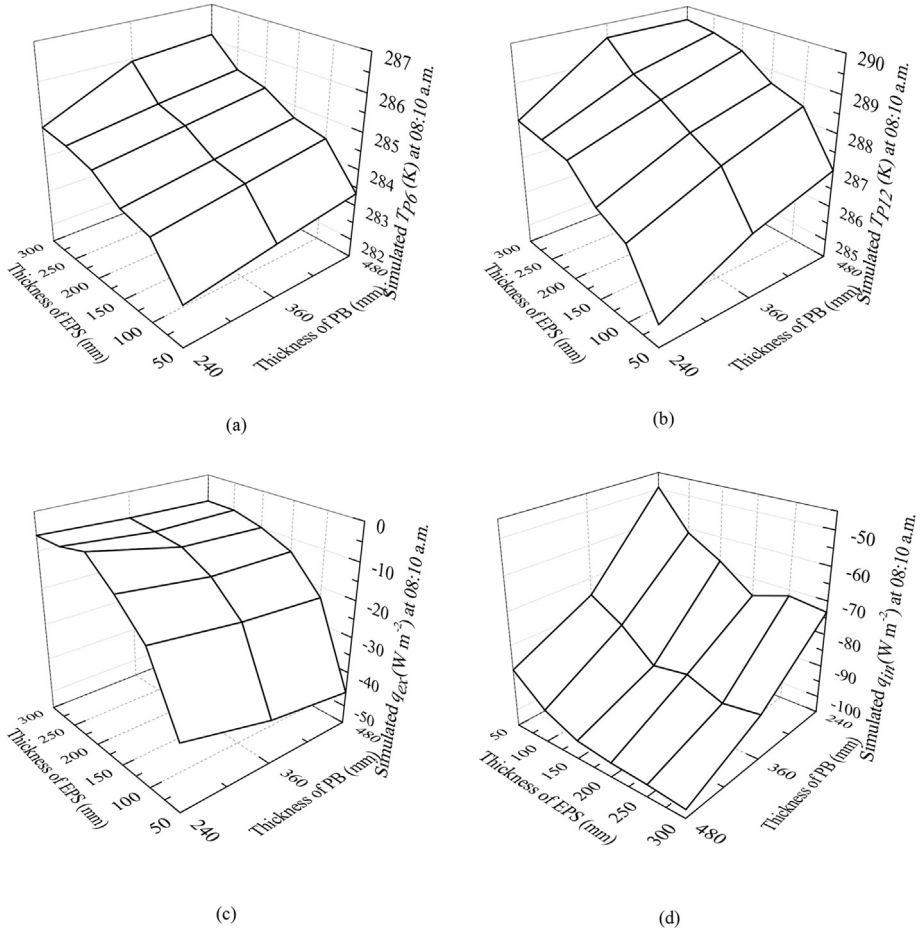

Fig. 11 – Simulated average (a) inside air temperature, (b) interior wall surface temperature, (c) q_{ex}, and (d) q_{in} distributions of 18 cases with varying thickness of perforated brick (PB) and expanded polystyrene board (EPS) north walls at 8:10 on January 26th, 2013.

changed dramatically when the thickness of EPS was increasing from 50 mm to 200 mm but slowly thereafter. The absolute value of q_{ex} increased due to increased heat loss when the thickness of EPS was kept constant but that of PB increased. Only if the EPS was thick enough, would the heat loss be reduced when the appropriate thickness of PB was used. The q_{in} for the thickest case was almost double that for the thinnest case (Fig. 11d). There was a similar pattern when the thickness of PB gradually increased and the thickness of EPS was 50 mm, 100 mm or 150 mm. According to the simulated data, q_{in} decreased when the thickness of EPS increased from 200 mm to 250 mm and that of PB was kept at 240 mm. The reason might be that the PB is the main conductive medium when the interior surface of north wall releases the thermal energy to the indoor air (Wang et al., 2014) and obviously 240 mm is too thin to maintain and conduct amounts of heat in terms of the temperature gradient. Although the EPS could insulate the heat energy from being lost to the outside air, q_{in} would not increase correspondingly and might even decrease. However, some results suggested that the 240 mm PB thickness could be sufficient for providing an acceptable energy performance in CSG (Li et al., 2009). Heat fluxes from soil (P3) and interior wall (P6) in 18 cases are shown in Fig. 12. The heat flux from soil was relatively small when compared to that from the interior wall, which also reasonably supports our simplifications proposed in Section 2.2.2.

3.4. *Rank result using optimized model*

Figure 13 illustrates the ranks of 18 simulation cases using weighted entropy and fuzzy optimisation method. The bigger the relative degree of membership means that the more cost-efficient is the case is better, and this can be used to automatically optimise the desired north wall across the cases. From results, cases 6 and 9 were observed to be the two most cost-efficient walls, suggesting 480 mm PB with 100 or 150 mm EPS to be appropriate for north walls.

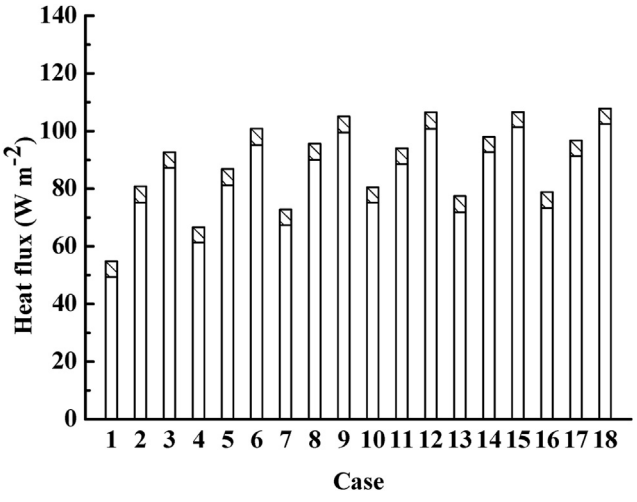

Fig. 12 – Heat flux contributions compared with soil surface (P3, ▨) and interior wall surface (P6, q_{in}, ▭) in 18 cases to support the last simplification.

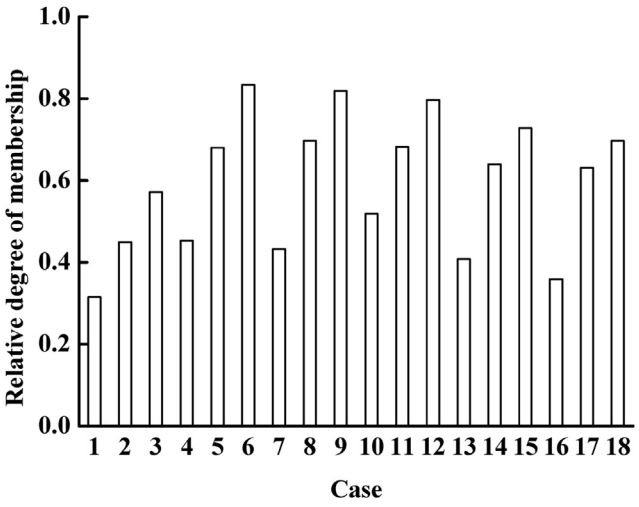

Fig. 13 – Ranks of 18 cases with relative degree of memberships using the comprehensive evaluation model.

4. Conclusions

A computer simulation model using the finite-volume-based commercial software Fluent® was used to evaluate the temperature distributions of CSG in winter nights. Experiments were conducted in a closed and empty CSG with two-layered north walls in northwest of China to validate the simulation model. The simulation results were in good agreement with the measured temperatures and simulations showed an obvious temperature gradient between PB and EPS, which suggested that EPS could preserve most of the thermal energy in PB. The validated computer simulation model was applied to predict temperature distributions in CSG with various thicknesses of north walls for 18 cases. Simulated results showed that the indoor temperature changed when the thickness of north walls were varied but the trends for temperature and heat flux were non-linear, indicating that there was a desirable thickness of north wall to meet the requirements for crop growth and for low cost at the same time. The temperature distribution within the CSG was relatively uniform because the temperatures at the measured locations followed the same change pattern during night. The comprehensive evaluation model using weighted entropy and fuzzy optimisation methods was an effective way to optimise the north walls based on their thickness and cost. Using the optimisation model, the two best choices satisfying adequate growing temperatures and reduced cost were north walls with 480 mm of PB and 100 or 150 mm of EPS. The developed simulation model is an effective tool to understand and analyse the complexity of thermal environments of CSG and improve temperature distributions using different thicknesses of north walls.

Acknowledgements

This research was conducted in College of Horticulture, Northwest A&F University, and supported by research grants

from Special Fund for Agro-Scientific Research in the Public Interest of Ministry of Agriculture of China (201203002). We thank all members of Agricultural Engineering Lab for their helps and Engineer at ANSYS Inc., Mr. Genong Li, for his remotely technical support. We also thank Associate Professor Kai Li in College of Water Resources and Architectural Engineering, Northwest A&F University, for his academic advices.

REFERENCES

Abdel-Ghany, A. M., & Kozai, T. (2006). On the determination of the overall heat transmission coefficient and soil heat flux for a fog cooled, naturally ventilated greenhouse: analysis of radiation and convection heat transfer. *Energy Conversion and Management, 47*(15–16), 2612–2628.

ANSYS, F. (2011). *User guide 14.0* (Lebanon, NH, USA).

Bartzanas, T., Boulard, T., & Kittas, C. (2004). Effect of vent arrangement on windward ventilation of a tunnel greenhouse. *Biosystems Engineering, 88*(4), 479–490.

Bierkens, J., & Kappen, H. J. (2014). Explicit solution of relative entropy weighted control. *Systems & Control Letters, 72*, 36–43.

Boulard, T., Kittas, C., Roy, J. C., & Wang, S. (2002). Convective and ventilation transfers in greenhouses, Part 2: determination of the distributed greenhouse climate. *Biosystems Engineering, 83*(2), 129–147.

Boulard, T., Lamrani, M. A., Roy, J. C., Jaffrin, A., & Bouirden, L. (1998). Natural ventilation by thermal effect in a one-half scale model mono-span greenhouse. *Transactions of the ASAE, 41*(3), 773–781.

Boulard, T., & Wang, S. (2002). Experimental and numerical studies on the heterogeneity of crop transpiration in a plastic tunnel. *Computers and Electronics in Agriculture, 34*(1–3), 173–190.

Chen, Q. (2008). Progress of practice and theory in sunlight greenhouse. *Journal of Shanghai Jiaotong University (Agricultural Science), 26*(5), 343–350.

De Luca, A., & Termini, S. (1972). A definition of a nonprobabilistic entropy in the setting of fuzzy sets theory. *Information and Control, 20*(4), 301–312.

Demirel, B. (2013). Optimization of the composite brick composed of expanded polystyrene and pumice blocks. *Construction and Building Materials, 40*, 306–313.

Fang, S., & Gao, Y. (2004). Research on thickness design of the layer of external insulation complet wall with EPS. *Journal of Heilongjiang Institute of Technology (Natural Science Edition), 18*(1), 57–59.

Fatnassi, H., Boulard, T., Poncet, C., & Chave, M. (2006). Optimisation of greenhouse insect screening with computational fluid dynamics. *Biosystems Engineering, 93*(3), 301–312.

Guiaşu, S. (1971). Weighted entropy. *Reports on Mathematical Physics, 2*(3), 165–179.

Guo, S., Sun, J., Shu, S., Lu, X., Tian, J., & Wang, J. (2012). Analysis of general situation, characteristics, existing problems and development trend of protected horticulture in China. *China Vegetables, 18*, 1–14.

Ji, Y., Huang, G. H., & Sun, W. (2015). Risk assessment of hydropower stations through an integrated fuzzy entropy-weight multiple criteria decision making method: a case study of the Xiangxi River. *Expert Systems with Applications, 42*(12), 5380–5389.

Jing, L., Ng, M. K., & Huang, J. Z. (2007). An entropy weighting k-means algorithm for subspace clustering of high-dimensional sparse data. *IEEE Transactions on Knowledge & Data Engineering, 19*(8), 1026–1041.

Jin, F., Pei, L., Chen, H., & Zhou, L. (2014). Interval-valued intuitionistic fuzzy continuous weighted entropy and its application to multi-criteria fuzzy group decision making. *Knowledge-Based Systems, 59*, 132–141.

Kang, S. (1990). Development and improvement for Chinese solar greenhouse of Anshan. *Transactions of the CSAE, 6*(2), 101–102.

Kobayashi, K., & Salam, M. U. (2000). Comparing simulated and measured values using mean squared deviation and its components. *Agronomy Journal, 92*(2), 345–352.

Lacarrière, B., Trombe, A., & Monchoux, F. (2006). Experimental unsteady characterization of heat transfer in a multi-layer wall including air layers—application to vertically perforated bricks. *Energy and Buildings, 38*(3), 232–237.

Lamrani, M. A. (1997). *Characterisation and modeling of the natural laminar and turbulent convection and ventilation in a greenhouse (in French)* (Ph.D. thesis). Agadir, Morocco: University of Agadir.

Lee, I.-B., Bitog, J. P. P., Hong, S.-W., Seo, I.-H., Kwon, K.-S., Bartzanas, T., et al. (2013). The past, present and future of CFD for agro-environmental applications. *Computers and Electronics in Agriculture, 93*, 168–183.

Lee, I.-B., Sase, S., & Sung, S.-H. (2007). Evaluation of CFD accuracy for the ventilation study of a naturally ventilated broiler house. *Japan Agricultural Research Quarterly, 41*(1), 53.

Li, J., Bai, Q., & Zhang, Y. (2010). Analysis on measurement of heat absorption and release of wall and ground in solar greenhouse. *Transactions of the CSAE, 26*(4), 231–236.

Li, X., & Chen, Q. (2006). Effects of different wall materials on the performance of heat preservation of wall of sunlight greenhouse. *Chinese Journal of Eco-Agriculture, 14*(4), 185–189.

Li, Y., & Hu, Y. (2006). A model of multilevel fuzzy comprehensive evaluation for investment risk of high and new technology project. In *Machine Learning and Cybernetics, 2006 International Conference on IEEE* (pp. 1942–1947) (Dalian, China).

Li, C., Li, Y., & Wen, X. (2009). Temperature characteristics of North Wall covered by polystyrene plate outside solar greenhouse. *Journal of Shanxi Agricultural University (Natural Science Edition), 29*(5), 453–457.

Lin, Z., Wen, F., & Zhou, H. (2009). Entropy weight based decision-making theory and its application to black-start decision-making. *Proceedings of the CSU EPSA, 21*(6), 26–33.

Majdoubi, H., Boulard, T., Fatnassi, H., & Bouirden, L. (2009). Airflow and microclimate patterns in a one-hectare Canary type greenhouse: an experimental and CFD assisted study. *Agricultural and Forest Meteorology, 149*(6–7), 1050–1062.

Mirsadeghi, M., Cóstola, D., Blocken, B., & Hensen, J. L. M. (2013). Review of external convective heat transfer coefficient models in building energy simulation programs: implementation and uncertainty. *Applied Thermal Engineering, 56*(1–2), 134–151.

Mistriotis, A., Arcidiacono, C., Picuno, P., Bot, G. P. A., & Scarascia-Mugnozza, G. (1997). Computational analysis of ventilation in greenhouses at zero- and low-wind-speeds. *Agricultural and Forest Meteorology, 88*(1–4), 121–135.

Molina-Aiz, F. D., Fatnassi, H., Boulard, T., Roy, J. C., & Valera, D. L. (2010). Comparison of finite element and finite volume methods for simulation of natural ventilation in greenhouses. *Computers and Electronics in Agriculture, 72*(2), 69–86.

Muñoz, P., Montero, J., Anton, A., & Iglesias, N. (2004). Computational fluid dynamic modelling of night-time energy fluxes in unheated greenhouses. *Acta Horticulturae, 691*, 403–410.

Norton, T., Sun, D.-W., Grant, J., Fallon, R., & Dodd, V. (2007). Applications of computational fluid dynamics (CFD) in the modelling and design of ventilation systems in the agricultural industry: a review. *Bioresource Technology, 98*(12), 2386–2414.

Qi, F. (2005). The conditions & trends of Chinese greenhouse and equipment industry. *Acta Agriculturae Shanghai, 21*(1), 53–57.

Qin, S. (2003). *Principle and application of comprehensive evaluation*. Beijing: Publishing House of Electronics Industry.

Qi, Y., Wen, F., Wang, K., Li, L., & Singh, S. (2010). A fuzzy comprehensive evaluation and entropy weight decision-making based method for power network structure assessment. *International Journal of Engineering, Science and Technology, 2*(5), 92–99.

Sase, S., Takakura, T., & Nara, M. (1983). Wind tunnel testing on airflow and temperature distribution of a naturally ventilated greenhouse. In *III International Symposium on Energy in Protected Cultivation 148* (pp. 329–336) (Columbus, USA).

Seo, I.-H., Lee, I.-B., Moon, O.-K., Hong, S.-W., Hwang, H.-S., Bitog, J. P., et al. (2012). Modelling of internal environmental conditions in a full-scale commercial pig house containing animals. *Biosystems Engineering, 111*(1), 91–106.

Swinbank, W. C. (1963). Long-wave radiation from clear skies. *Quarterly Journal of the Royal Meteorological Society, 89*(381), 339–348.

Teferra, K., Shields, M. D., Hapij, A., & Daddazio, R. P. (2014). Mapping model validation metrics to subject matter expert scores for model adequacy assessment. *Reliability Engineering & System Safety, 132*, 9–19.

Tong, G., & Christopher, D. (2009). Simulation of temperature variations for various wall materials in Chinese solar greenhouses using computational fluid dynamics. *Transactions of the CSAE, 25*(3), 153–157.

Tong, G., Christopher, D., & Li, B. (2009). Numerical modelling of temperature variations in a Chinese solar greenhouse. *Computers and Electronics in Agriculture, 68*(1), 129–139.

Tong, G., Christopher, D., Li, T., & Wang, T. (2013). Passive solar energy utilization: a review of cross-section building parameter selection for Chinese solar greenhouses. *Renewable and Sustainable Energy Reviews, 26*, 540–548.

Tong, G., Christopher, D., Zhao, R., Wang, J., & Zhang, Y. (2014). Temperature variations in Chinese solar greenhouses with different wall material thicknesses. *Xinjiang Agricultural Sciences, 51*(6), 999–1007.

Tong, G., Li, B., Christopher, D., & Yamaguchi, T. (2007). Preliminary study on temperature pattern in China solar greenhouse using computational fluid dynamics. *Transactions of the CSAE, 23*(7), 178–185.

Versteeg, H. K., & Malalasekera, W. (1995). *An introduction to computational fluid dynamics*. London: Longman Group Ltd.

Wang, Q., Chen, J., Sun, Z., Zhao, Y., Wu, M., Yang, X., et al. (2010). Heat flux analysis of inner surface of north wall in solar greenhouse. *Chinese Journal of Agrometeorology, 31*(2), 225–229.

Wang, J., Li, S., Guo, S., Ma, C., Wang, J., & Jin, S. (2014). Simulation and optimization of solar greenhouses in Northern Jiangsu Province of China. *Energy and Buildings, 78*, 143–152.

Wang, X., Luo, J., & Li, X. (2013). CFD based study of heterogeneous microclimate in a typical Chinese greenhouse in central China. *Journal of Integrative Agriculture, 12*(5), 914–923.

Wei, X., Qi, F., Ding, X., Bao, S., Li, Z., & He, F. (2010). Main achievements in China facility horticulture. *Journal of Agricultural Mechanization Research, 32*(12), 227–231.

Wu, J., & Zhang, Q. (2011). Multicriteria decision making method based on intuitionistic fuzzy weighted entropy. *Expert Systems with Applications, 38*(1), 916–922.

Yang, Q. (2012). Energy efficient heating technologies and models in lean-to Chinese solar greenhouses: a review. In *IV International Symposium on Models for Plant Growth, Environmental Control and Farm Management in Protected Cultivation* (pp. 83–89) (Nanjing, China).

Yang, J., Zou, Z., Zhang, Z., Wang, Y., Zhang, Z., & Yan, F. (2009). Optimization of earth wall thickness and thermal insulation property of solar greenhouse in Northwest China. *Transactions of the CSAE, 25*(8), 180–185.

Zadeh, L. A. (1968). Probability measures of fuzzy events. *Journal of Mathematical Analysis and Applications, 23*(2), 421–427.

Zerihun Desta, T., Janssens, K., Van Brecht, A., Meyers, J., Baelmans, M., & Berckmans, D. (2004). CFD for model-based controller development. *Building and Environment, 39*(6), 621–633.

Zhang, S., Zhang, M., & Chi, G. (2010). The science and technology evaluation model based on entropy weight and empirical research during the10th five-year of China. *Chinese Journal of Management, 7*(1), 34–42.

Zhou, H., Zhang, G., & Wang, G. (2007). Multi-objective decision making approach based on entropy weights for reservoir flood control operation. *Journal of Hydraulic Engineering, 38*(1), 100–106.